# Resolving Quantum Interference Black Box through Attosecond Photoionization Spectroscopy

Wenyu Jiang,[1] Gregory S. J. Armstrong,[2] Lulu Han,[1] Yidan Xu,[1] Zitan Zuo,[1] Jihong Tong,[1] Peifen Lu,[1] Jan Marcus Dahlström,[3] Kiyoshi Ueda,[1,4] Andrew C. Brown,[2,*] Hugo W. van der Hart,[2] Xiaochun Gong,[1,5,†] and Jian Wu[1,5,6,7,‡]

[1]*State Key Laboratory of Precision Spectroscopy, East China Normal University, Shanghai 200241, China*
[2]*Centre for Light-Matter Interaction, School of Mathematics and Physics, Queen's University Belfast, Belfast BT7 1NN, Northern Ireland, United Kingdom*
[3]*Department of Physics, Lund University, P.O. Box 118, 22100 Lund, Sweden*
[4]*Department of Chemistry, Tohoku University, Sendai 980-8578, Japan*
[5]*Collaborative Innovation Center of Extreme Optics, Shanxi University, Taiyuan, Shanxi 030006, China*
[6]*Chongqing Key Laboratory of Precision Optics, Chongqing Institute of East China Normal University, Chongqing 401121, China*
[7]*CAS Center for Excellence in Ultra-intense Laser Science, Shanghai 201800, China*

(Received 9 May 2023; revised 30 August 2023; accepted 13 October 2023; published 14 November 2023)

Multiphoton light-matter interactions invoke a so-called "black box" in which the experimental observations contain the quantum interference between multiple pathways. Here, we employ polarization-controlled attosecond photoelectron metrology with a partial wave manipulator to deduce the pathway interference within this quantum 'black box" for the two-photon ionization of neon atoms. The angle-dependent and attosecond time-resolved photoelectron spectra are measured across a broad energy range. Two-photon phase shifts for each partial wave are reconstructed through the comprehensive analysis of these photoelectron spectra. We resolve the quantum interference between the degenerate $p \to d \to p$ and $p \to s \to p$ two-photon ionization pathways, in agreement with our theoretical simulations. Our approach thus provides an attosecond time-resolved microscope to look inside the "black box" of pathway interference in ultrafast dynamics of atoms, molecules, and condensed matter.

DOI: 10.1103/PhysRevLett.131.203201

When multiple transition pathways are available to create photoelectrons in the same final state, the phase and transition amplitude of each individual pathway is hidden from experimental measurement. The accessible observable includes the interference between the different pathways, which results in a so-called quantum "black box" [1]. This pathway interference plays a fundamental role in light-matter interaction [2], most famously in two-center or double-slit interference [3–5]. This paradigm has been used to interpret many phenomena including Cohen-Fano photoelectron emission time delays [6], attosecond photoelectron holography [7], electron localization in a molecule [8,9], quantum trajectory interference in high-order harmonic generation [10,11], and even zeptosecond scale electron birth time [12]. Experimentally, the fingerprints of this (quantum) pathway interference can be found in (photoelectron) momentum observations [1,3], or in oscillations within a measured signal in the (delay) time domain.

Modern attosecond metrology has enabled the measurement of the phase shift of a photoelectron wave packet passing through the potential well of its parent ion [13–18]. This metrology has opened a new avenue to investigate photoelectron emission dynamics on their natural timescale, and has been exploited to study asymmetric molecular orbit effects in photoelectron emission [19,20], shape resonances [21–24], two-center interference [5], circular dichroism of electron vortices [25] and electron delocalizations [16]. For photoionization delay studies, attosecond pulse trains (APT) in the extreme ultraviolet (XUV) region are employed and the photoionization phase shift measurement realized using the RABBITT (reconstruction of attosecond beating by interference of two-photon transitions) approach [26,27].

In RABBITT studies, a sideband (SB) electron arises from the interference between two ionization pathways. One involves the absorption of a near-infrared (NIR) photon and its $(2q-1)$th harmonic XUV photon, and another involves the absorption of one $(2q+1)$th harmonic XUV photon and emission of one NIR photon. Their interference manifests itself as an oscillation in the yield as a function of the pump-probe delay. The SB oscillation encodes the two-photon phase shift between the absorption and emission pathways, and its phase is defined as $\phi^{\mathrm{SB}} = \Delta\phi^{2h\nu} + \Delta\phi_{\mathrm{XUV}}$, where $\Delta\phi_{\mathrm{XUV}}$ is the attochirp of the XUV-APT [28], and the two-photon phase shift is $\Delta\phi^{2h\nu} = \Delta\phi_{\mathrm{EWS}} + \Delta\phi_{\mathrm{cc}}$. $\Delta\phi_{\mathrm{EWS}}$ is related to the Eisenbud-Wigner-Smith time delay between adjacent high harmonics [29,30], and $\Delta\phi_{\mathrm{cc}}$ is the continuum-continuum transition phase shift between two

 

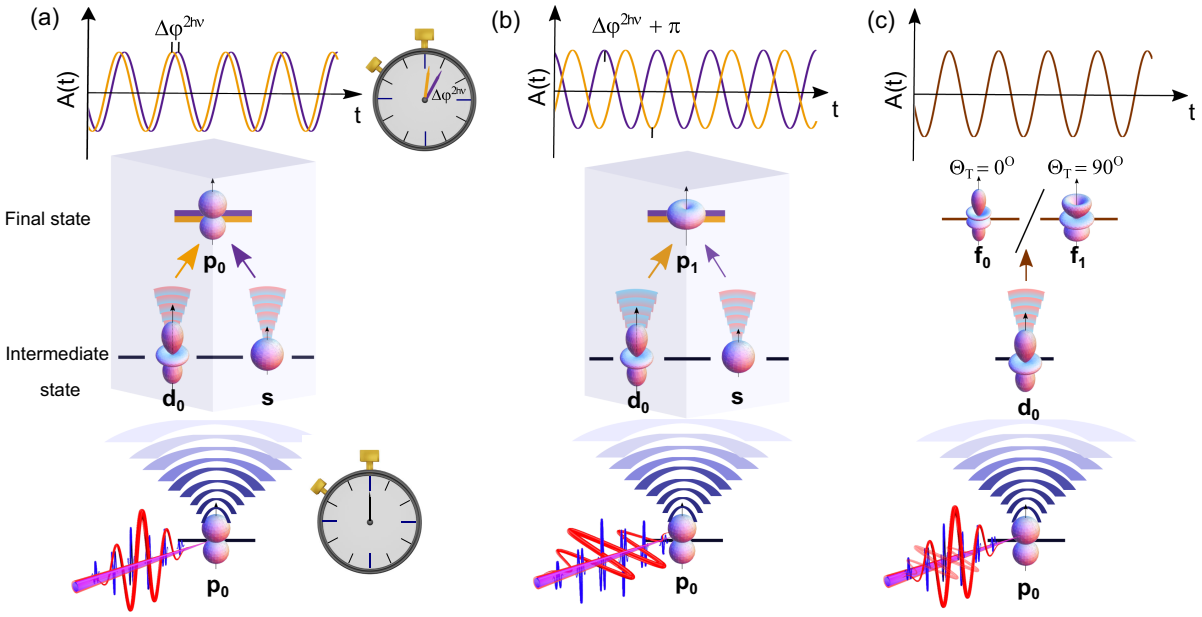


FIG. 1. (a) Schematic diagram of two-photon XUV + NIR quantum transition pathway at $\Theta_T = 0°$. The final $p_0$ wave originates from the coherent superposition between pathway $p_0 \to s \to p_0$ and pathway $p_0 \to d_0 \to p_0$ from the same initial $p_0$ electron. (b) Same as (a) but for $\Theta_T = 90°$ following the quantum transition pathways of $p_0 \to s \to p_{\pm 1}$ and $p_0 \to d_0 \to p_{\pm 1}$. The yellow and purple lines indicate the transition pathway through the intermediate state of $d$ and $s$ waves, respectively. (c). The sketch for the polarization-independent transition pathways of $p_0 \to d_0 \to f_0$ at $\Theta_T = 0°$ and $p_0 \to d_0 \to f_{\pm 1}$ at $\Theta_T = 90°$.

pathways induced by the long-range Coulomb potential in the NIR field [31,32]. Experimental observations [17,33,34] demonstrate that, for simple systems such as helium, the characteristics of each partial wave, identified by the electron orbital angular momentum $l$ and magnetic quantum number $m$, including the amplitude ratios and phase shifts, can be reconstructed for every single partial-wave absorption or emission pathway based on the angle-resolved photoelectron phase shifts [18,23,35–37].

As illustrated in Fig. 1, the photoelectron wave packet generated by two-photon ionization in neon is created through three distinct transition pathways: $p \to s \to p$, $p \to d \to p$, and $p \to d \to f$. The final $p$ wave may be reached via two intermediate states—$s$ or $d$—but the observable encodes only their interference. This, then, is a pathway interference "black box," where, in principle, the which-way information is hidden from the observer. Here, we demonstrate the decomposition of this interference "black box" by employing polarization-controlled XUV-APT and NIR attosecond coincidence metrology to realize a symmetry-resolved photoionization experiment.

Experimentally, we observe both the symmetry-resolved photoelectron angular distributions and angle-resolved phase shift distributions induced by the NIR field at each sideband for neon atoms. The polarization axis of the weak NIR field is tuned with a cross angle ($\Theta_T$) set at 0° or 90°. An *ab initio* simulation using the R-matrix-with-time-dependence (RMT) method was also performed to obtain theoretical yields and phase shifts for each partial wave [38–40]. The measurements from two different skew angles, 0° and 90°, provide sufficient information to reconstruct the separate magnitudes and phases of the $p \to d \to p$ and $p \to s \to p$ pathways from the measured spectra, and the results are in good agreement with the theoretical predictions from RMT.

The XUV-APT is prepared via high harmonic generation in an Ar gas-filled capillary, covering high harmonics from 20.41 eV (H13) to 36.1 eV (H23). Three-dimensional momenta of ion fragments and photoelectrons are measured in coincidence using a cold target recoil ion momentum spectroscopy setup [41,42]. See Fig. S1 in the Supplemental Material (SM) for more details [43]. By varying the time delay $\tau$ between the XUV-APT and the NIR field, the SB yields oscillate as $Y_{SB} = A\cos(2\omega_{NIR}\tau - \phi^{SB}) + B$, where $\omega_{NIR}$ is the angular frequency of the NIR field [32,49]. To aid comparison between phase shifts for different SBs, we then compute the SB phase shift difference, $\Delta\phi^{SB}_{rel}(\theta) = \phi^{SB}(\theta) - \phi^{SB}(\theta = \Theta_T)$.

Figures 2(a)–2(c) show the SB phase shift difference of neon atoms at $\Theta_T = 0°$ as a function of electron emission angle and kinetic energy. The $\Delta\phi^{SB16}_{rel}$ in Fig. 2(a) presents a strong emission angle dependence [50]. Moving from an emission angle of 0° to 50° induces a relative phase shift of $-0.085\pi$, and we observe a phase jump of approximately $\pi$ radians at the node of the photoelectron angular distribution at $\theta = 90°$. For higher-order sidebands [Figs. 2(b) and 2(c)], $\Delta\phi^{SB}_{rel}$ varies more slowly as $\theta$ deviates from 0°. For $\Theta_T = 90°$, the same flattening of the phase shift with increasing kinetic energy is observed, although the phase jumps are now centered on $\theta = 0°$.

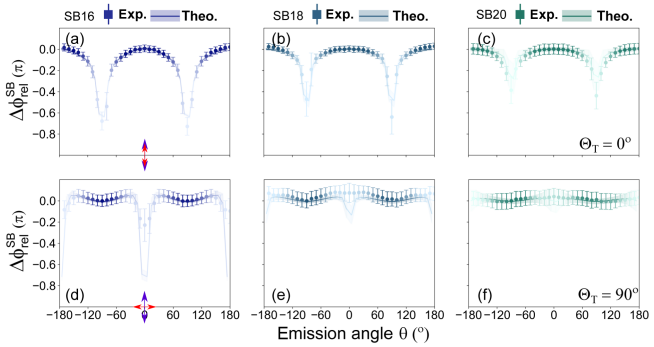


FIG. 2. (a)–(c) Angle-resolved relative two-photon phase shift distributions of (a) SB16 (3.53 eV), (b) SB18 (6.70 eV), and (c) SB20 (9.84 eV) in neon atoms at $\Theta_T = 0°$, where the purple and red arrows indicate the polarization axis of the XUV and NIR laser fields. The squares show the experimental results with standard deviation. The solid lines represent the theoretical simulations with a shaded area indicating the standard deviation. The opacity is weighted by the photoelectron yields. (d)–(f) Same as (a)–(c) but for $\Theta_T = 90°$. The discrepancy between theory and experiment at 0° in (d) and (e) is attributed to the low photoelectron yield at these emission angles and the limited angular resolution in the experimental results compared to the (theoretical perfect) angular resolution in the RMT results.

To understand the kinetic energy dependence of each $\Delta\phi_{\mathrm{rel}}^{\mathrm{SB}}$ and to further clarify the transition pathway superposition, we performed RMT simulations and extracted the two-photon phase shifts, $\phi_{lm}^{2h\nu}$, for each partial wave and each residual-ion state (ionization of neon may leave the residual ion in either the $P_0$ or $P_{\pm1}$ states). Figures 3(a)–3(c) present the resulting $\phi_{lm}^{2h\nu}$ for neon as a function of electron kinetic energy at $\Theta_T = 0°$, and Figs. 3(d)–3(f) for $\Theta_T = 90°$. In most cases, the two-photon phase shifts for the partial waves vary only slightly with kinetic energy and are almost identical to each other. The exceptions are the $p_0$ and $p_{\pm1}$ waves associated with the $P_0$ ionic state. The kinetic energy dependence for $p_{\pm1}$ is still rather slight, but for $p_0$, $\phi_{p_0}^{2h\nu}$ increases from $-0.48\pi$ to $-0.12\pi$ between SB16 and SB22, corresponding to a photoemission time delay of 236 as. Importantly, these two—the $p_0$ and $p_{\pm1}$ waves—can arise from two intermediate states, $s$ or $d_0$. By contrast, all partial waves that arise from a single intermediate state display an almost flat phase shift with kinetic energy. We use these partial waves as a reference to determine the quantum-number dependence of the phase shifts, which is required to resolve the interference "black box" in the $p$ waves. Figure 4(a) shows how this can be accomplished, namely by taking differences between the phases of partial waves arising from the same $d_{\pm1}$ intermediate state.

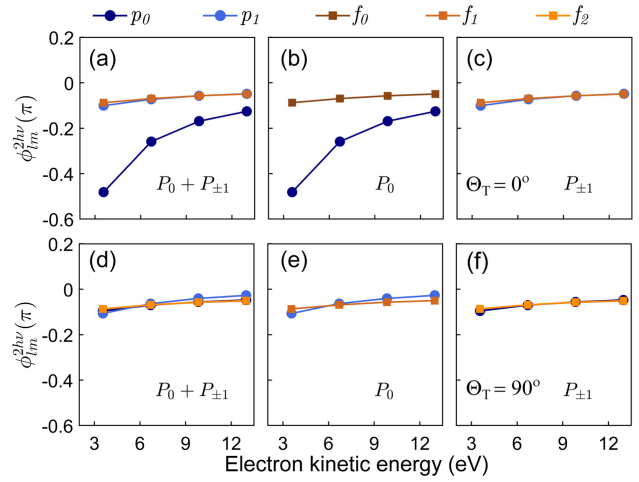


FIG. 3. (a)–(c) Partial wave resolved two-photon phase shift $\phi_{lm}^{2h\nu}$ of photoelectrons coupled to the residual ionic state of (a) the incoherent sum of $P_0$ and $P_{\pm1}$, (b) $P_0$, and (c) $P_{\pm1}$ at $\Theta_T = 0°$. The blue color weighted circle lines represent the results of $p_0$ and $p_{\pm1}$ waves, and the orange color weighted square lines show $f_0$, $f_{\pm1}$, and $f_{\pm2}$, respectively. (d)–(f). Same as (a)–(c) but for results at $\Theta_T = 90°$.

Figure 4(b) presents the differences between two-photon phase shifts for $p$ and $f$ waves with the same magnetic quantum number, $m$, calculated using RMT. A slight difference between $f$ and $p$ waves is observed at low energy. Since they pass through a common $d_{\pm1}$ intermediate state, the phase difference must result directly from the continuum-continuum transitions. In other words, $\Delta\phi_{\mathrm{cc}}$ does depend on $l$. If instead we compare final states with common orbital angular momentum $l$ for different skew angles in Fig. 4(c), the differences between $p_{\pm1}$ and $p_0$, and between $f_{\pm1}$ and $f_0$ are almost zero, i.e., $\Delta\phi_{\mathrm{cc}}$ does not depend on $m$. Coupled with the fact that the two-photon phase shifts for $f_0$ and $f_{\pm1}$ at $\Theta_T = 0°$ are identical, this indicates that the Wigner-phase shifts $\Delta\phi_{\mathrm{EWS}}$ are also independent of the magnetic quantum number, $m$. This is

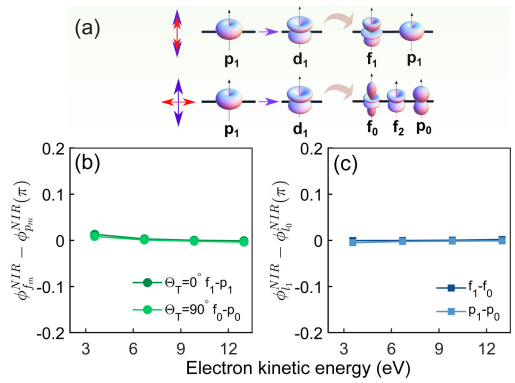


FIG. 4. (a) Sketch of the two-photon transition pathway of the electron coupled to the $P_{\pm1}$-residual ionic state for $\Theta_T = 0°$ and 90°. (b) Theoretically calculated continuum-continuum phase shift difference between $f$ and $p$ waves with the same magnetic quantum number. The dark and light green lines show the results for $m = \pm1$ and $m = 0$. (c) Same as (b) but for $m$-resolved continuum-continuum phase shift difference. The dark and light blue lines represent the phase shift difference between $f_{\pm1}$ and $f_0$, and $p_{\pm1}$ and $p_0$ waves.

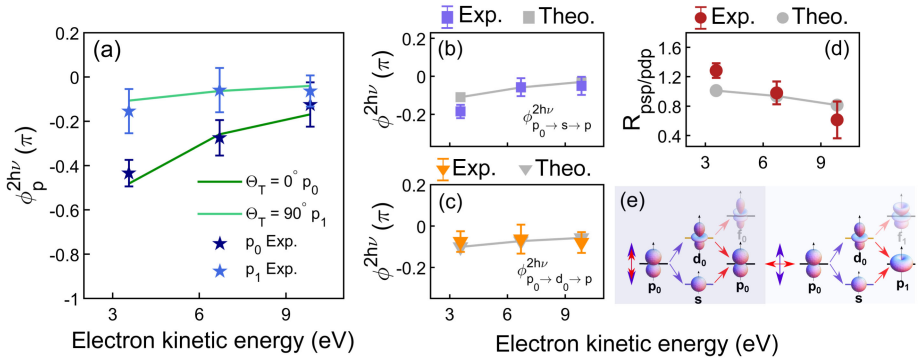


FIG. 5. (a) Reconstructed electron kinetic energy dependent two-photon phase shift $\phi^{2h\nu}_{p_0}$ and $\phi^{2h\nu}_{p_1}$ at $\Theta_T = 0°$ and 90°, respectively. (b),(c) Intermediate state resolved two-photon phase shift of (b) $\phi^{2h\nu}_{p_0\to s\to p}$ and (c) $\phi^{2h\nu}_{p_0\to d_0\to p}$. (d) Amplitude ratio between $p_0 \to s \to p_0$ and $p_0 \to d_0 \to p_0$ at $\Theta_T = 0°$. The theoretical and experimental results are shown in lines and discrete labels. (e) Sketch of the two-photon transition pathway for electron coupled to the same final state at $\Theta_T = 0°$ and $\Theta_T = 90°$.

critical for the resolution of the pathway interference (see SM [43]).

The kinetic energy dependence observed for the $p_0$ wave at $\Theta_T = 0°$ and $p_{\pm1}$-wave at 90° are manifestations of the interference between two ionization pathways via $s$- and $d_0$-intermediate states. Figure 5(a) shows reconstructed two-photon phase shifts of $p_0$ and $p_{\pm1}$ waves under the laser field geometry of $\Theta_T = 0°$ and 90° from the experimentally measured $\Delta\phi^{SB}_{rel}$ distributions shown in Fig. 2. The reconstruction method is described in detail in the SM [43]. Based on the "soft photon approximation," at $\Theta_T = 0°$ the interference can be described analytically as [17,51,52]

$$R^{0°}_{interf} e^{-i\phi^{2h\nu}_{p_0}} = \frac{R_{ps}}{3} e^{-i\phi^{2h\nu}_{psp}} - \frac{4R_{pd}}{15} e^{-i\phi^{2h\nu}_{pdp}}, \quad (1)$$

where the $(R_{ps}/3)$ and $(4R_{pd}/15)$ are the transition amplitudes from $p_0 \to s \to p_0$ and $p_0 \to d_0 \to p_0$, and $\phi^{2h\nu}_{psp}$ and $\phi^{2h\nu}_{pdp}$ are the two-photon phase shifts associated with each transition pathway. At $\Theta_T = 90°$, the interference is

$$R^{90°}_{interf} e^{-i\phi^{2h\nu}_{p_{\pm1}}} = \frac{1}{\sqrt{2}} \frac{R_{ps}}{3} e^{-i\phi^{2h\nu}_{psp}} + \frac{\sqrt{2}R_{pd}}{15} e^{-i\phi^{2h\nu}_{pdp}}. \quad (2)$$

Here, the $R_{ps}$ and $R_{pd}$ represent the XUV induced radial transition amplitude for each intermediate state that is not affected by the polarization of the NIR field. The perpendicularly polarized NIR field works as a phase manipulator introducing an additional $\pi$ phase shift between the two ionization pathways. This changes the sign of the $R_{pd}$ contribution to the total transition matrix element and is analogous to double-slit interference but with two different intermediate slits. The kinetic energy resolved $\phi^{2h\nu}_{p_0}$ at $\Theta_T = 0°$, $\phi^{2h\nu}_{p_{\pm1}}$ at $\Theta_T = 90°$, and $\phi^{2h\nu}_{pdp}$ are reconstructed from the experimental $\Delta\phi^{2h\nu}_{rel}$ distributions, where the $\phi^{2h\nu}_{pdp}$ is equal to $\phi^{2h\nu}_{p_{\pm1}}$ at $\Theta_T = 0°$. Thus the hidden "which-way" information, namely the relative transition amplitude between the two interference pathways and the two-photon phase shifts of the $p_0 \to s \to p_{0,\pm1}$ pathway can be resolved by solving Eqs. (1) and (2) simultaneously (more details in SM [43]).

In essence, then, the experiment measures the difference and sum of the two pathways, and from these we may reconstruct the two-photon phase shifts and amplitudes of each pathway. Figures 5(b) and 5(c) show the two-photon phase shifts for the individual pathways reconstructed from the RMT simulations and experimental measurements. Figure 5(d) displays the reconstructed relative transition amplitude between the $p_0 \to s \to p_0$ and $p_0 \to d_0 \to p_0$ pathways for $\Theta_T = 0°$. In all cases, the reconstructed results from experiment agree with the theoretical simulations.

As shown in Figs. 5(b) and 5(c), the reconstructed two-photon phase shifts $\phi^{2h\nu}_{psp}$ and $\phi^{2h\nu}_{pdp}$ are similar, and both gradually approach zero as a function of electron kinetic energy. Nevertheless, we see significant differences between the kinetic energy dependence of the $p_0$ channel at $\Theta_T = 0°$, and of the $p_{\pm1}$ channel at $\Theta_T = 90°$. This contrast can be explained through the sign difference in Eqs. (1) and (2). With similar phases for the two components and constructive interference, the $p_{\pm1}$ channel at $\Theta_T = 90°$ follows the behavior of the individual pathways. However, for $\Theta_T = 0°$, in the $p_0$ channel the two components interfere destructively. This pathway puts far more emphasis on the phase difference between the two components, and we see this phase difference amplified in Fig. 5(a). As a result, although the XUV-APT induced relative one-photon transition amplitude $R_{s/d}$ is independent of the laser field geometry, the energy dependence of $\phi^{2h\nu}_{p_{\pm1}}$ at $\Theta_T = 90°$ is different to that of $\phi^{2h\nu}_{p_0}$ at $\Theta_T = 0°$, as shown in Figs. 3(a) and 3(d).

In summary, we demonstrate the decomposition of quantum interference within the two-photon ionization of neon atoms by employing a polarization-controlled attosecond photoelectron metrology. Our partial wave analysis

reconstructs the pathway-resolved two-photon phase shifts of final $p$ waves between the two interfering pathways: $\phi^{2h\nu}_{p\to s\to p}$ and $\phi^{2h\nu}_{p\to d\to p}$. Our experimental results agree well with the RMT simulations and illustrate that the energy dependence is dominated by the decreased phase shift difference between $p$ and $f$ waves as a function of the electron energy. For photoelectrons associated with the $P_0$-residual ionic state, the parallel and perpendicular geometry induces a $\pi$ phase jump between $s$- and $d_0$-intermediate states, analogous to the ungerade and gerade type interference in double-slit interference, which results in the large photoemission phase shifts in different polarization states. Our experimental and theoretical study establishes a connection between the experimental observable and the underlying partial wave characters and reveals the interference effect of two-photon transition pathways via different intermediate states under different polarization geometries. It provides a new perspective to probe and control the ultrafast photoelectron dynamics in atoms, molecules, and condensed matter involving the multichannel interference phenomena, like Fano resonance [12,53], giant resonance [54], shape resonance [23,55], and Cooper minimum [56].

This work was supported by the National Natural Science Foundation of China (Grants No. 12241407, No. 12122404, No. 12261160363, No. 11974114, No. 12227807, No. 11834004), the Science and Technology Commission of Shanghai Municipality (Grant No. 228002246), and the Fundamental Research Funds for the Central Universities (Grant No. YBNLTS2023-010). G. A., A. B., and H. v.-d.-H. acknowledge the work from Daniel D. A. Clarke and Jakub Benda in developing new capabilities within the RMT code that were used in this work, and the funding from the UK Engineering and Physical Sciences Research Council (EPSRC) under Grants No. EP/T019530/1, No. EP/V05208X/1, and No. EP/R029342/1. This work relied on the ARCHER2 UK Supercomputer Service, for which access was obtained via the UK-AMOR consortium funded by EPSRC. The RMT code is part of the UK Atomic, Molecular and Optical physics R-matrix (UK-AMOR) suite. This work benefited from computational support by CoSeC, the Computational Science Centre for Research Communities, through CCPQ. J. M. D. acknowledges support from the Swedish Research Council: 2018-03845, the Olle Engkvist Foundation: 194-0734 and the Knut and Alice Wallenberg Foundation: 2017.0104 and 2019.0154.

*andrew.brown@qub.ac.uk
†xcgong@lps.ecnu.edu.cn
‡jwu@phy.ecnu.edu.cn

[1] S. Dürr, T. Nonn, and G. Rempe, Fringe visibility and which-way information in an atom interferometer, Phys. Rev. Lett. **81**, 5705 (1998).
[2] H. D. Cohen and U. Fano, Interference in the photoionization of molecules, Phys. Rev. **150**, 30 (1996).
[3] M. Kunitski, N. Eicke, P. Huber, J. Köhler, S. Zeller, J. Voigtsberger, N. Schlott, K. Henrichs, H. Sann, F. Trinter, L. P. H. Schmidt, A. Kalinin, M. S. Schöf, T. Jahnke, M. Lein, and R. Dörner, Double-slit photoelectron interference in strong-field ionization of the neon dimer, Nat. Commun. **10**, 1 (2019).
[4] X.-J. Liu, Q. Miao, F. Gel'mukhanov, M. Patanen, O. Travnikova, C. Nicolas, H. Ågren, K. Ueda, and C. Miron, Einstein–Bohr recoiling double-slit gedanken experiment performed at the molecular level, Nat. Photonics **9**, 120 (2015).
[5] S. Heck, M. Han, D. Jelovina, J.-b. Ji, C. Perry, X. Gong, R. Lucchese, K. Ueda, and H. J. Wörner, Two-center interference in the photoionization delays of Kr2, Phys. Rev. Lett. **129**, 133002 (2022).
[6] M. Kotur, D. Guénot, Jiménez-Galán, D. Kroon, E. W. Larsen, M. Louisy, S. Bengtsson, M. Miranda, J. Mauritsson, C. L. Arnold, S. E. Canton, M. Gisselbrecht, T. Carette, J. M. Dahlström, E. Lindroth, A. Maquet, L. Argenti, F. Martín, and A. L'Huillier, Spectral phase measurement of a Fano resonance using tunable attosecond pulses, Nat. Commun. **7**, 10566 (2016).
[7] G. Porat, G. Alon, S. Rozen, O. Pedatzur, M. Krüger, D. Azoury, A. Natan, G. Orenstein, B. D. Bruner, M. J. Vrakking, and N. Dudovich, Attosecond time-resolved photoelectron holography, Nat. Commun. **9**, 2805 (2018).
[8] M. F. Kling, A. J. Verhoef, J. I. Khan, M. Schultze, Y. Ni, M. Uiberacker, M. Drescher, F. Krausz, and M. J. J. Vrakking, Control of electron localization in molecular dissociation, Science **312**, 246 (2006).
[9] G. Sansone *et al.*, Electron localization following attosecond molecular photoionization, Nature (London) **465**, 763 (2010).
[10] A. Zaïr, M. Holler, A. Guandalini, F. Schapper, J. Biegert, L. Gallmann, U. Keller, A. S. Wyatt, A. Monmayrant, I. A. Walmsley, E. Cormier, T. Auguste, J. P. Caumes, and P. Salières, Quantum path interferences in high-order harmonic generation, Phys. Rev. Lett. **100**, 143902 (2008).
[11] F. Schapper, M. Holler, T. Auguste, A. Zaïr, M. Weger, P. Salières, L. Gallmann, and U. Keller, Spatial fingerprint of quantum path interferences in high order harmonic generation, Opt. Express **18**, 2987 (2010).
[12] V. Gruson, L. Barreau, Jiménez-Galan, F. Risoud, J. Caillat, A. Maquet, B. Carré, F. Lepetit, J. F. Hergott, T. Ruchon, L. Argenti, R. Taïeb, F. Martín, and P. Salières, Attosecond dynamics through a Fano resonance: Monitoring the birth of a photoelectron, Science **354**, 734 (2016).
[13] J. Itatani, F. Quéré, G. L. Yudin, M. Y. Ivanov, F. Krausz, and P. B. Corkum, Attosecond streak camera, Phys. Rev. Lett. **88**, 173903 (2002).
[14] E. Goulielmakis, M. Uiberacker, R. Kienberger, A. Baltuska, V. Yakovlev, A. Scrinzi, T. Westerwalbesloh, U. Kleineberg, U. Heinzmann, M. Drescher, and F. Krausz, Direct measurement of light waves, Science **305**, 1267 (2004).
[15] M. Schultze *et al.*, Delay in photoemission, Science **328**, 1658 (2010).
[16] X. Gong, S. Heck, D. Jelovina, C. Perry, K. Zinchenko, R. Lucchese, and H. J. Wörner, Attosecond spectroscopy of

size-resolved water clusters, Nature (London) **609**, 507 (2022).
[17] W. Jiang, G. S. Armstrong, J. Tong, Y. Xu, Z. Zuo, J. Qiang, P. Lu, D. D. Clarke, J. Benda, A. Fleischer, H. Ni, K. Ueda, H. W. van der Hart, A. C. Brown, X. Gong, and J. Wu, Atomic partial wave meter by attosecond coincidence metrology, Nat. Commun. **13**, 5072 (2022).
[18] J. Peschel, D. Busto, M. Plach, M. Bertolino, M. Hoflund, S. Maclot, J. Vinbladh, H. Wikmark, F. Zapata, E. Lindroth, M. Gisselbrecht, J. M. Dahlström, A. L'Huillier, and P. Eng-Johnsson, Attosecond dynamics of multi-channel single photon ionization, Nat. Commun. **13**, 5205 (2022).
[19] J. Vos, L. Cattaneo, S. Patchkovskii, T. Zimmermann, C. Cirelli, M. Lucchini, A. Kheifets, A. S. Landsman, and U. Keller, Orientation-dependent stereo Wigner time delay and electron localization in a small molecule, Science **360**, 1326 (2018).
[20] J. Rist *et al.*, Measuring the photoelectron emission delay in the molecular frame, Nat. Commun. **12**, 6657 (2021).
[21] M. Huppert, I. Jordan, D. Baykusheva, A. Von Conta, and H. J. Wörner, Attosecond delays in molecular photoionization, Phys. Rev. Lett. **117**, 093001 (2016).
[22] S. Nandi, E. Plésiat, S. Zhong, A. Palacios, D. Busto, M. Isinger, L. Neoričić, C. L. Arnold, R. J. Squibb, R. Feifel, P. Decleva, A. L'Huillier, F. Martín, and M. Gisselbrecht, Attosecond timing of electron emission from a molecular shape resonance, Sci. Adv. **6**, eaba7762 (2020).
[23] X. Gong, W. Jiang, J. Tong, J. Qiang, P. Lu, H. Ni, R. Lucchese, K. Ueda, and J. Wu, Asymmetric attosecond photoionization in molecular shape resonance, Phys. Rev. X **12**, 011002 (2022).
[24] F. Holzmeier, J. Joseph, J. C. Houver, M. Lebech, D. Dowek, and R. R. Lucchese, Influence of shape resonances on the angular dependence of molecular photoionization delays, Nat. Commun. **12**, 7343 (2021).
[25] M. Han, J.-B. Ji, T. Balčiūnas, K. Ueda, and H. J. Wörner, Attosecond circular-dichroism chronoscopy of electron vortices, Nat. Phys. **19**, 230 (2022).
[26] P. M. Paul, E. S. Toma, P. Breger, G. Mullot, F. Augé, P. Balcou, H. G. Muller, and P. Agostini, Observation of a train of attosecond pulses from high harmonic generation, Science **292**, 1689 (2001).
[27] Y. Mairesse, A. De Bohan, I. J. Frasinski, H. Merdji, L. C. Dinu, P. Monchicourt, P. Breger, M. Kovačev, R. Taïeb, B. Carré, H. G. Muller, P. Agostini, and P. Salières, Attosecond synchronization of high-harmonic soft x-rays, Science **302**, 1540 (2003).
[28] K. Varjú, Y. Mairesse, B. Carré, M. B. Gaarde, P. Johnsson, S. Kazamias, R. López-Martens, J. Mauritsson, K. J. Schafer, P. Balcou, A. L'Huillier, and P. Salières, Frequency chirp of harmonic and attosecond pulses, J. Mod. Opt. **52**, 379 (2005).
[29] E. P. Wigner, Lower limit for the energy derivative of the scattering phase shift, Phys. Rev. **98**, 145 (1955).
[30] F. T. Smith, Lifetime matrix in collision theory, Phys. Rev. **118**, 349 (1960).
[31] A. Harth, N. Douguet, K. Bartschat, R. Moshammer, and T. Pfeifer, Extracting phase information on continuum-continuum couplings, Phys. Rev. A **99**, 023410 (2019).
[32] J. M. Dahlström, D. Guénot, K. Klünder, M. Gisselbrecht, J. Mauritsson, A. L'Huillier, A. Maquet, and R. Taïeb, Theory of attosecond delays in laser-assisted photoionization, Chem. Phys. **414**, 53 (2013).
[33] L. H. Haber, B. Doughty, and S. R. Leone, Continuum phase shifts and partial cross sections for photoionization from excited states of atomic helium measured by high-order harmonic optical pump-probe velocity map imaging, Phys. Rev. A **79**, 031401(R) (2009).
[34] J. Fuchs, N. Douguet, S. Donsa, F. Martin, J. Burgdorfer, L. Argenti, L. Cattaneo, and U. Keller, Time delays from one-photon transitions in the continuum, Optica **7**, 154 (2020).
[35] A. Autuori, D. Platzer, M. Lejman, G. Gallician, L. Maëder, A. Covolo, L. Bosse, M. Dalui, D. Bresteau, J. F. Hergott, O. Tcherbakoff, H. J. Marroux, V. Loriot, F. Lépine, L. Poisson, R. Taïeb, J. Caillat, and P. Salières, Anisotropic dynamics of two-photon ionization: An attosecond movie of photoemission, Sci. Adv. **8**, eabl7594 (2022).
[36] S. Heuser, Á. J. Galán, C. Cirelli, C. Marante, M. Sabbar, R. Boge, M. Lucchini, L. Gallmann, I. Ivanov, A. S. Kheifets, J. M. Dahlström, E. Lindroth, L. Argenti, F. Martín, and U. Keller, Angular dependence of photoemission time delay in helium, Phys. Rev. A **94**, 063409 (2016).
[37] A. W. Bray, F. Naseem, and A. S. Kheifets, Simulation of angular-resolved RABBITT measurements in noble-gas atoms, Phys. Rev. A **97**, 063404 (2018).
[38] L. R. Moore, M. A. Lysaght, L. A. A. Nikolopoulos, J. S. Parker, H. W. van der Hart, and K. T. Taylor, The RMT method for many-electron atomic systems in intense short-pulse laser light, J. Mod. Opt. **58**, 1132 (2011).
[39] H. W. van der Hart, M. A. Lysaght, and P. Burke, Momentum distributions of electrons ejected during ultrashort laser interactions with multielectron atoms described using the r-matrix basis sets, Phys. Rev. A **77**, 065401 (2008).
[40] A. C. Brown, G. S. J. Armstrong, J. Benda, D. D. A. Clarke, J. Wragg, K. R. Hamilton, Z. Mašín, J. D. Gorfinkiel, and H. W. van der Hart, RMT: R-matrix with time-dependence. Solving the semi-relativistic, time-dependent Schrödinger equation for general, multielectron atoms and molecules in intense, ultrashort, arbitrarily polarized laser pulses, Comput. Phys. Commun. **250**, 107062 (2020).
[41] R. Dörner, V. Mergel, O. Jagutzki, L. Spielberger, J. Ullrich, R. Moshammer, and H. Schmidt-Böcking, Cold target recoil ion momentum spectroscopy: A 'momentum microscope' to view atomic collision dynamics, Phys. Rep. **330**, 95 (2000).
[42] J. Ullrich, R. Moshammer, A. Dorn, R. Dörner, L. P. H. Schmidt, and H. Schmidt-Böcking, Recoil-ion and electron momentum spectroscopy: Reaction-microscopes, Rep. Prog. Phys. **66**, 1463 (2003).
[43] See Supplemental Material at http://link.aps.org/supplemental/10.1103/PhysRevLett.131.203201 for the experimental and theoretical method, the reconstruction of the sideband phase shifts and partial wave resolved two-photon phase shifts, the decomposition of the quantum transition interference, the ionic state resolved photoelectron angular distributions, and relative two-photon phase shift distributions, which includes Refs. [44–48].
[44] J. Ladislas Wiza, Microchannel plate detectors, Nucl. Instrum. Methods **162**, 587 (1979).

[45] O. Jagutzki, A. Cerezo, A. Czasch, R. Dörner, M. Hattaß, M. Huang, V. Mergel, U. Spillmann, K. Ullmann-Pfleger, T. Weber, H. Schmidt-Böcking, and G. D. Smith, Multiple hit readout of a microchannel plate detector with a three-layer delay-line anode, IEEE Trans. Nucl. Sci. **49 II**, 2477 (2002).

[46] D. D. A. Clarke, G. S. J. Armstrong, A. C. Brown, and H. W. van der Hart, *r*-matrix-with-time-dependence theory for ultrafast atomic processes in arbitrary light fields, Phys. Rev. A **98**, 053442 (2018).

[47] P. G. Burke and K. T. Taylor, R-matrix theory of photoionization. Application to neon and argon, J. Phys. B **8**, 2620 (1975).

[48] A. S. Kheifets, Symmetry analysis of the photoelectron continuum in two-photon XUV + IR ionization, Phys. Rev. A **105**, 013114 (2022).

[49] J. M. Dahlström, A. L'Huillier, and A. Maquet, Introduction to attosecond delays in photoionization, J. Phys. B **45**, 183001 (2012).

[50] I. A. Ivanov and A. S. Kheifets, Angle-dependent time delay in two-color XUV + IR photoemission of He and Ne, Phys. Rev. A **96**, 013408 (2017).

[51] A. Maquet and R. Taïeb, Two-colour IR + XUV spectroscopies: The "soft-photon approximation", J. Mod. Opt. **54**, 1847 (2007).

[52] D. Guénot, D. Kroon, E. Balogh, E. W. Larsen, M. Kotur, M. Miranda, T. Fordell, P. Johnsson, J. Mauritsson, M. Gisselbrecht, K. Varjú, C. L. Arnold, T. Carette, A. S. Kheifets, E. Lindroth, A. L'Huillier, and J. M. Dahlström, Measurements of relative photoemission time delays in noble gas atoms, J. Phys. B **47**, 245602 (2014).

[53] C. Cirelli *et al.*, Anisotropic photoemission time delays close to a Fano resonance, Nat. Commun. **9**, 955 (2018).

[54] A. D. Shiner, B. E. Schmidt, C. Trallero-Herrero, H. J. Wörner, S. Patchkovskii, P. B. Corkum, J.-C. Kieffer, F. Légaré, and D. M. Villeneuve, Probing collective multielectron dynamics in xenon with high-harmonic spectroscopy, Nat. Phys. **7**, 464 (2011).

[55] S. Heck, D. Baykusheva, M. Han, J.-B. Ji, C. Perry, X. Gong, and H. J. Wörner, Attosecond interferometry of shape resonances in the recoil frame of CF4, Sci. Adv. **7**, eabj8121 (2021).

[56] C. Alexandridi, D. Platzer, L. Barreau, D. Busto, S. Zhong, M. Turconi, L. Neoričić, H. Laurell, C. L. Arnold, A. Borot, J. F. Hergott, O. Tcherbakoff, M. Lejman, M. Gisselbrecht, E. Lindroth, A. L'Huillier, J. M. Dahlström, and P. Salières, Attosecond photoionization dynamics in the vicinity of the Cooper minima in argon, Phys. Rev. Res. **3**, L012012 (2021).